Euler–Lagrange Optimal Control for Symmetric Projectiles

Bradley T. Burchett*and Austin L. Nash†
Rose-Hulman Institute of Technology, Terre Haute, IN, 47803

The linear theory model of a symmetric projectile is well suited to optimal control methods, especially the finite horizon linear optimal regulator. Using a nine–state linear model with gravity treated as an uncontrollable mode, necessary conditions for optimality are derived. These conditions are solved closed–form using a matrix exponential of the Hamiltonian matrix multiplied by distance to go in calibers. Control is thus found without a reference trajectory. A second method allowing system parameters to vary with time is developed and compared. The time–varying Riccati equation is solved recursively backward in time and control at the current state is found without a reference trajectory. Performance is demonstrated on linear and non–linear plant models using forward mounted canards.

Nomenclature

$\mathbf{P}$, $\mathbf{Q}$, $\mathbf{R}$	optimal control weighting matrices
$\mathbf{A}, \mathbf{B}$	Linear State Space Matrices
C_{NA}	normal force aerodynamic coefficient
C_{X0}	axial force aerodynamic coefficient
C_{LP}	roll rate damping moment aerodynamic coefficient
C_{LDD}	fin rolling moment aerodynamic coefficient
C_{MA}	pitch moment due to AOA aerodynamic coefficient
C_{MQ}	pitch rate damping moment aerodynamic coefficient
D	projectile characteristic length (ft)
g	gravitational constant = 32.2 (ft/s^2)
$\mathbf{I}$	identity matrix
I_{xx}, I_{yy}	roll and pitch inertia expressed in the projectile reference frame (sl-ft^2)
m	projectile mass (sl)
p, q, r	angular velocity vector components expressed in the fixed plane reference frame (rad/s)
S	$= \pi D^2/4$, projectile reference area (ft^2)
SL_{cg}	stationline of the projectile c.g. location (ft)
SL_{cp}	stationline of the projectile c.p. location (ft)
s	downrange distance (calibers)
u, v, w	translation velocity components of the projectile center of mass resolved in the fixed plane reference frame (ft/s)
V	$= \sqrt{u^2+v^2+w^2}$, magnitude of the mass center velocity (ft/s)
x, y, z	position vector components of the projectile mass center expressed in the inertial reference frame (ft)
Greek	
$\mathbf{\Sigma}_{ij}$	state transition matrices
ρ	air density (sl/ft^3)
ψ, θ, ϕ	Euler yaw, pitch, and roll angles (rad)
$\mathbf{\Xi}$	velocity state vector dynamics matrix

*Associate Professor, Department of Mechanical Engineering, burchett@rose-hulman.edu, Associate Fellow, AIAA
†Graduate Research Assistant, Department of Mechanical Engineering, nashal@rose-hulman.edu

ξ linear model position state vector $\{\ y \quad z \quad \theta \quad \psi\ \}^T$
η linear model velocity state vector $\{\ v \quad w \quad q \quad r\ \}^T$
σ $= s - s_t$, distance to go (calibers)

Subscript
t target

I. Introduction

In recent years, the control of symmetric projectiles has largely been implemented using Model Predictive Control (MPC).[1,2,3,4] Methods range from predicting the impact point with and without control, to converting the plant dynamics to a discrete time system, and providing a desired trajectory to the target. Using the customary flat–fire projectile linear theory model, an optimal control problem can be formulated without the need for prediction, reference trajectories, or discrete time conversions. In this work, the need for a reference trajectory is eliminated by 1) removing the state penalty term from the cost function, and 2) treating gravity as an uncontrollable mode. The result is a continuous time finite horizon Euler–Lagrange optimal controller. Performance of the controller will be demonstrated on a six DOF non–linear simulation of a symmetric projectile with moveable canards.

II. Model Dynamics and Control

The projectile yaw–swerve and epicyclic pitch–yaw equations of motion may be collected into a nine-dimensional linear state space description as shown in Eq. (1). For a complete development of the linear model see references [2],[6],[7],[10] or [11]. In order to conform to the antecedents of linear optimal control, the uncontrollable state $\dot{w}$ is appended with initial condition $\dot{w}(0) = Dg/V$, thus treating gravity g as an uncontrollable mode. Four canards are mounted in an axially symmetric fashion, and two control inputs correspond to the lift coefficients of planar pairs of canards $\{C_{Y0},\ C_{Z0}\}$ that act along the y and z directions in the projectile no–roll frame.

$$\begin{Bmatrix} \dot{\xi} \\ \dot{\eta} \\ \ddot{w} \end{Bmatrix} = \begin{bmatrix} \mathbf{\Phi} & \mathbf{\Gamma} & \mathbf{0} \\ \mathbf{0} & \mathbf{\Xi} & \mathbf{\Lambda} \\ \mathbf{0} & \mathbf{0} & 0 \end{bmatrix} \begin{Bmatrix} \xi \\ \eta \\ \dot{w} \end{Bmatrix} + \begin{bmatrix} \mathbf{0} \\ \mathbf{b} \\ \mathbf{0} \end{bmatrix} \begin{Bmatrix} C_{Z0} \\ C_{Y0} \end{Bmatrix} \tag{1}$$

or

$$\dot{\mathbf{x}} = \mathbf{A}\mathbf{x} + \mathbf{B}\mathbf{u}$$

Where

$$\xi = \begin{bmatrix} y & z & \theta & \psi \end{bmatrix}^T,\ \eta = \begin{bmatrix} v & w & q & r \end{bmatrix}^T,\ \mathbf{\Lambda} = \begin{bmatrix} 0 & 1 & 0 & 0 \end{bmatrix}^T,\ \mathbf{\Gamma} = \frac{D}{V}\mathbf{I}$$

$$\mathbf{\Phi} = \begin{bmatrix} 0 & 0 & 0 & D \\ 0 & 0 & -D & 0 \\ 0 & 0 & 0 & 0 \\ 0 & 0 & 0 & 0 \end{bmatrix},\ \mathbf{\Xi} = \begin{bmatrix} -\Xi_1 & 0 & 0 & -D \\ 0 & -\Xi_1 & D & 0 \\ \Xi_2 & \Xi_3 & \Xi_4 & -\Xi_5 \\ -\Xi_3 & \Xi_2 & \Xi_5 & \Xi_4 \end{bmatrix}$$

and

$$\Xi_1 = \frac{\rho S D}{2m} C_{NA} \tag{2}$$

$$\Xi_3 = \frac{\rho S D}{2I_{yy}} C_{MA} \tag{3}$$

$$\Xi_4 = \frac{\rho S D^3}{4I_{yy}} C_{MQ} \tag{4}$$

$$\Xi_5 = \frac{D}{V}\frac{I_{xx} p}{I_{yy}} \tag{5}$$

$$C_{MA} = (SL_{COP} - SL_{CG}) C_{NA} \tag{6}$$

$\mathbf{\Xi}_2$ is the Magnus term

$$\mathbf{\Xi}_2 = \frac{\rho S}{2m}\frac{mD}{I_{yy}}\frac{D}{V}(SL_{cm} - SL_{cg})C_{NPA}p$$

and D is the projectile characteristic length (or diameter). The epicyclic state control matrix is

$$\mathbf{b} = \begin{bmatrix} 0 & -b_1 & b_2 & 0 \\ b_1 & 0 & 0 & b_2 \end{bmatrix}^T$$

where

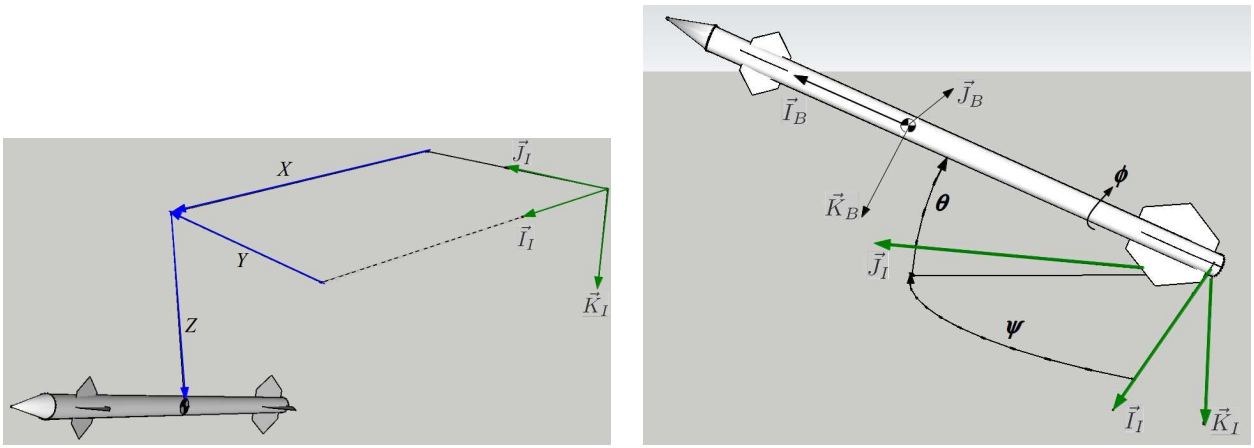

(a) Position (b) Angle

Figure 1. Coordinate Definitions for the Rocket with Canards

$$\begin{aligned} b_1 &= \frac{\rho S_{can} D}{2m} V \\ b_2 &= \frac{\rho S_{can} D}{2I_{yy}} V(3.8 - SL_{cg}) \end{aligned} \tag{7}$$

The total velocity V and spin rate p are treated as parameters in the state equations above. As the projectile moves downrange, they also vary and may be modeled by the following ODEs.

$$\dot{V} = -\frac{\rho S D}{2m} C_{X0} V$$

$$\dot{p} = \frac{\rho S D^3 C_{LP}}{4I_{xx}} p + \frac{\rho S D^2 V}{2I_{xx}} C_{LDD}$$

II.A. Linear Time Invariant (LTI) Optimal Regulator

Since the projectile yaw/swerve position and epicyclic pitch/yaw states may be written as a 9th order linear, time varying plant model (Eq. (1)), necessary conditions for optimality may be formed as follows. The cost function is chosen as

$$J = \frac{1}{2}\mathbf{x}^T(s_t)\mathbf{P}\mathbf{x}(s_t) + \int_{s_i}^{s_t} \frac{1}{2}\mathbf{x}^T\mathbf{Q}\mathbf{x} + \mathbf{u}^T\mathbf{R}\mathbf{u}\, ds$$

Since $\mathbf{Q}$ is required only to be semi-definite, we choose $\mathbf{Q} = 0$, thus eliminating the need for a reference trajectory. The state dynamics of Eq. (1) serve as equality constraints.

The corresponding Hamiltonian function is

$$\tilde{H} = \frac{1}{2}\mathbf{u}^T\mathbf{R}\mathbf{u} + \lambda^T(\mathbf{A}\mathbf{x} + \mathbf{B}\mathbf{u})$$

The Euler-Lagrange equations are

$$\begin{aligned} \dot{\lambda}^T &= -\frac{\partial \tilde{H}}{\partial \mathbf{x}} = -\lambda^T \mathbf{A} \\ \frac{\partial \tilde{H}}{\partial \mathbf{u}} &= \mathbf{0} \rightarrow \mathbf{0} = \mathbf{u}^T \mathbf{R} + \lambda^T \mathbf{B} \end{aligned}$$

or

$$\mathbf{R}\mathbf{u} + \mathbf{B}^T \lambda = \mathbf{0},$$

and

$$\lambda(s_t) = \mathbf{P}\mathbf{x}(s_t) \tag{8}$$

where s_i is the initial downrange arclength in calibers and s_t is the downrange arclength at the target. Choosing $\mathbf{R} > 0$, the control is found to be

$$\mathbf{u} = -\mathbf{R}^{-1}\mathbf{B}^T \lambda \tag{9}$$

Substituting this feedback law into the state equations and concatenating the state and costate equations, the $2n \times 2n$ system is obtained.

$$\left\{ \begin{array}{c} \dot{\mathbf{x}} \\ \dot{\lambda} \end{array} \right\} = \left[\begin{array}{cc} \mathbf{A} & -\mathbf{B}\mathbf{R}^{-1}\mathbf{B}^T \\ \mathbf{0} & -\mathbf{A}^T \end{array} \right] \left\{ \begin{array}{c} \mathbf{x} \\ \lambda \end{array} \right\} \tag{10}$$

Substituting the linear mapping between state and costate at the target range s_t (Eq. (8)), the $2n \times 2n$ system may be solved using state transition matrices $\mathbf{\Sigma}_{ij}$.

$$\left\{ \begin{array}{c} \mathbf{x}(s) \\ \lambda(s) \end{array} \right\} = \left[\begin{array}{cc} \mathbf{\Sigma}_{11} & \mathbf{\Sigma}_{12} \\ \mathbf{\Sigma}_{21} & \mathbf{\Sigma}_{22} \end{array} \right] \left\{ \begin{array}{c} \mathbf{x}(s_t) \\ \mathbf{P}\mathbf{x}(s_t) \end{array} \right\}$$

such that

$$\mathbf{x}(s) = \left(\mathbf{\Sigma}_{11} + \mathbf{\Sigma}_{12}\mathbf{P}\right) \mathbf{x}(s_t)$$

or

$$\mathbf{x}(s_t) = \left(\mathbf{\Sigma}_{11} + \mathbf{\Sigma}_{12}\mathbf{P}\right)^{-1} \mathbf{x}(s)$$

and since

$$\lambda(s) = \left(\mathbf{\Sigma}_{21} + \mathbf{\Sigma}_{22}\mathbf{P}\right) \mathbf{x}(s_t)$$

the co–state at downrange distance s is

$$\lambda(s) = \left[\mathbf{\Sigma}_{21} + \mathbf{\Sigma}_{22}\mathbf{P}\right] \bullet \left[\mathbf{\Sigma}_{11} + \mathbf{\Sigma}_{12}\mathbf{P}\right]^{-1} \mathbf{x}(s) \tag{11}$$

Where the state transition matrices can be found using the following matrix exponential

$$\left[\begin{array}{cc} \mathbf{\Sigma}_{11} & \mathbf{\Sigma}_{12} \\ \mathbf{\Sigma}_{21} & \mathbf{\Sigma}_{22} \end{array} \right] = \exp \left[\begin{array}{cc} \mathbf{A}\sigma & -\mathbf{B}\mathbf{R}^{-1}\mathbf{B}^T\sigma \\ \mathbf{0} & -\mathbf{A}^T\sigma \end{array} \right] \tag{12}$$

and $\sigma = s - s_t$ or distance to go in calibers. Note that despite the block Hessenberg form of the Hamiltonian matrix, the matrix exponential may not be taken in a piecewise fashion. Here the Pade algorithm by Van Loan[9] is used to numerically find the matrix exponential.

Eq. (12) has the effect of integrating the eqns. of motion forward along the trajectory, and simultaneously integrating the costate equation backward from the target. Thus, it makes an implicit trajectory prediction.

II.B. Time Varying Piecewise Linear Optimal Regulator

The previous method suffers from inaccuracies due to assuming that the roll rate p, and total velocity V are constant in the implicit trajectory prediction. In order to provide for the time varying nature of these parameters, a second method is investigated. The system matrices $(\mathbf{A}, \mathbf{B})$ become time varying ($\mathbf{A}(s)$, $\mathbf{B}(s)$) such that arclength travel downrange remains the independent variable. The control $\mathbf{u}$ is then

$$\mathbf{u}(s) = -\mathbf{R}^{-1}\mathbf{B}^T(s)\mathbf{N}(s)\mathbf{x}(s) \tag{13}$$

Where $\mathbf{N}(s)$ is the solution to the Riccati matrix differential equation:

$$\dot{\mathbf{N}}(s) = -\mathbf{N}(s)\mathbf{A}(s) - \mathbf{A}^T(s)\mathbf{N}(s) + \mathbf{N}(s)\mathbf{B}(s)\mathbf{R}^{-1}\mathbf{B}^T(s)\mathbf{N}(s) - \mathbf{Q} \tag{14}$$

and $\mathbf{Q} = 0$. Eq. (14) is decomposed into two matrix differential equations

$$\dot{\mathbf{W}}(s) = \mathbf{A}(s)\mathbf{W}(s) - \mathbf{B}(s)\mathbf{R}^{-1}\mathbf{B}^T(s)\mathbf{Y}(s) \tag{15}$$

$$\dot{\mathbf{Y}}(s) = -\mathbf{A}^T(s)\mathbf{Y}(s) \tag{16}$$

Target conditions $\mathbf{W}(s_t)$ and $\mathbf{Y}(s_t)$ are chosen according to the cost function

$$\begin{aligned} \mathbf{W}(s_t) &= \mathbf{I} \\ \mathbf{Y}(s_t) &= \mathbf{P} \end{aligned}$$

The matrix Riccati solution is then

$$\mathbf{N}(s) = \mathbf{Y}(s)\mathbf{W}(s)^{-1} \tag{17}$$

Eqs. (15) & (16) can be written in terms of a time varying Hamiltonian as $\dot{\mathbf{Z}}(s) = \mathbf{F}(s)\mathbf{Z}(s)$. That is:

$$\begin{Bmatrix} \dot{\mathbf{W}}(s) \\ \dot{\mathbf{Y}}(s) \end{Bmatrix} = \begin{bmatrix} \mathbf{A}(s) & -\mathbf{B}(s)\mathbf{R}^{-1}\mathbf{B}^T(s) \\ 0 & -\mathbf{A}^T(s) \end{bmatrix} \begin{Bmatrix} \mathbf{W}(s) \\ \mathbf{Y}(s) \end{Bmatrix} \tag{18}$$

In order to form the time varying Hamiltonian, roll rate and total velocity must be predicted from current position to target. The following closed form expressions may be used to do this recursively.[11]

$$p(s+h) = p(s)\Lambda + \frac{2V(s)C_{LDD}}{DC_{LP}} \exp\left(-\frac{\rho SDC_{X0}}{2m}h\right)(\Lambda - 1)$$

Where

$$\Lambda = \exp\left(\frac{\rho SD^3C_{LP}}{4I_{xx}}h\right)$$

and

$$V(s+h) = V(s)\exp\left(-\frac{\rho SDC_{X0}}{2m}h\right)$$

The time varying Riccati eqn. can be solved recursively by discretizing the trajectory into n_s segments from current position to target. The solution is then back propagated using:[12]

$$\mathbf{Z}_{n_s} = \left(\mathbf{I} + \frac{h}{2}\mathbf{F}_{n_s}\right)^{-1}\mathbf{Z}(s_t) \tag{19}$$

$$\mathbf{Z}_k = \left(\mathbf{I} + \frac{h}{2}\mathbf{F}_k\right)^{-1}\left(\mathbf{I} - \frac{h}{2}\mathbf{F}_{k+1}\right)\mathbf{Z}_{k+1},\ k = 0, 1, \ldots, n_s - 1 \tag{20}$$

The current control command $\mathbf{u}(s)$ is then computed using Eqs. (17) & (13).

Thus, in summary, the time varying algorithm is:

- Calculate the distance to target $|\sigma|$
- Divide this distance into n_s equal segments such that

$$h = |\sigma|/(n_s - 1)$$

- Recursively estimate total V and p updating aero coefficients at each segment
- Build the corresponding Hamiltonian matrix for each segment
- Integrate backwards in time using Eqs. (19) & (20)
- Use $\mathbf{Z}_1$ to compute Riccati solution at current state
- Use Eq. (13) to compute control in no roll frame

II.C. Non-linear Implementation

II.C.1. Transform Canard Commands to Roll Frame

Since the **b** matrix includes scaling due to dynamic pressure, canard area, and stationline moment arm, the controls found by Eq. (9) are in fact the non–dimensional canard force coefficients in the no–roll frame. In order to convert to a canard angle in the body frame, they must merely be converted to δ_{can} by a reverse table look–up, then rotated into the body frame. The rotation from no–roll NR to body frame R is simply

$$\left\{ \begin{array}{c} \delta_Z \\ \delta_Y \end{array} \right\}_R = \left[\begin{array}{cc} \cos\phi_c & \sin\phi_c \\ -\sin\phi_c & \cos\phi_c \end{array} \right] \left\{ \begin{array}{c} \delta_Z \\ \delta_Y \end{array} \right\}_{NR} . \tag{21}$$

Where δ_{YR} corresponds to the canard which will exert a lift force approximately along the $\hat{\jmath}_B$ axis for $\delta_C > 0$ as shown in Figure 2. The paired canard will have command $= -\delta_C$ in the canard frame such that coplanar canards are in phase to an outside observer. Simulations will initially only consider trajectories that remain supersonic throughout. In this case, the inverse table look–up is simply $\delta_{can}[\mathtt{rad}] = C_{Y0}/C_{L\alpha}$ where $C_{L\alpha} = 4.135[\mathtt{rad}]^{-1}$ for mach $M > 1$. The resulting canard angle is then limited such that $-1 < \delta_{can} < 1$. Note that local angle of attack is assumed to be negligible compared to commanded δ_{can}.

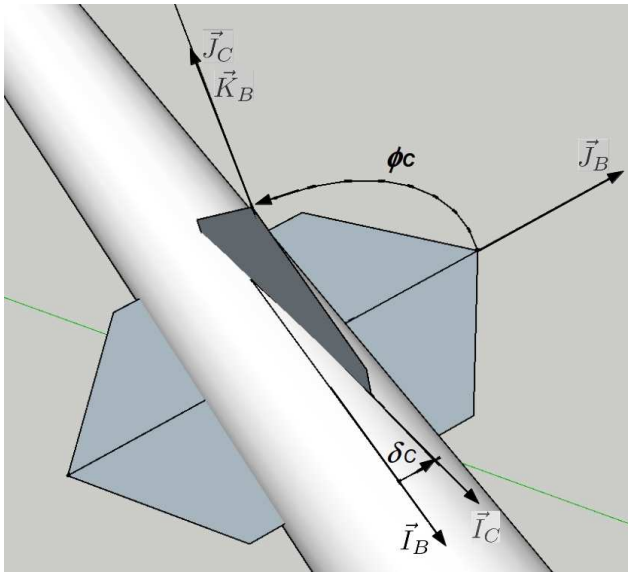

Figure 2. Canard Euler Angles Relative to the Body Frame

II.C.2. Vacuum Trajectory Correction

The linear model uses downrange distance in calibers, s as the independent variable. When driving a linear plant with the linear controller, s may be considered parallel to the downrange ($\hat{\imath}$) ground fixed axis. When porting the linear model to a non–linear plant, however, distance to go must be computed from actual arc length to be traveled along the trajectory. Thus a more accurate prediction of distance to go is sought.

One possibility is to find an intersecting point mass vacuum trajectory and use its arclength distance to go in place of the difference between target downrange and current downrange. In terms of time of flight, the point mass vacuum trajectory may be written

$$z = z_0 + V_{0z}t + \frac{a}{2}t^2 \tag{22}$$

$$x = V_{0x}t \tag{23}$$

Where in this context z is altitude positive up, and x is the downrange distance in the $x - z$ plane. Eq. (23) may be solved for time in terms of x, and substituted into the altitude equation, rendering altitude as a function of distance downrange.

$$z(x) = z_0 + V_{0z}\frac{x}{V_{0x}} + \frac{a}{2}\left(\frac{x}{V_{0x}}\right)^2 \tag{24}$$

The arclength to go may then be found by first invoking Pythagorean theorem as $ds = \sqrt{dx^2 + dz^2}$, and finding an expression for dz by differentiating Eq. (24) with respect to x.

$$dz = \left(\frac{V_{0z}}{V_{0x}} + \frac{a}{V_{0x}^2} x \right) dx \tag{25}$$

Substituting into Pythagorean theorem and simplifying, the differential arclength is found to be

$$ds = \sqrt{\left(\frac{V_{0z}}{V_{0x}} + \frac{a}{V_{0x}^2} x \right)^2 + 1} \; dx \tag{26}$$

Thus the arclength distance to go may be found by integrating from current downrange position to target

$$\int ds = \int_x^{x_t} \sqrt{\left(\frac{V_{0z}}{V_{0x}} + \frac{a}{V_{0x}^2} x \right)^2 + 1} \; dx \tag{27}$$

The integral results in a very lengthy expression which is presented in the appendix.

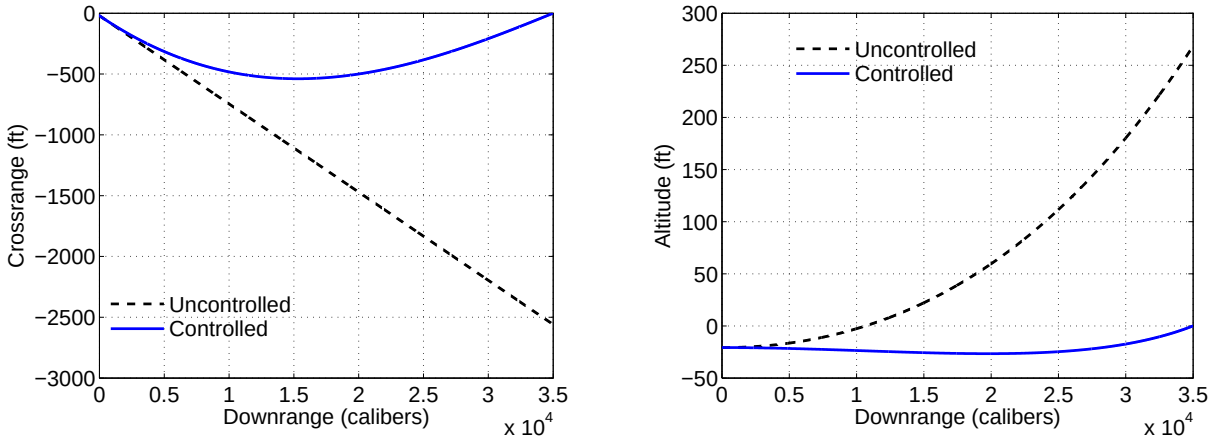

(a) Crossrange

(b) Altitude

Figure 3. Strategy I Controller Performance for Poorly Aimed Shot

The unknown parameters of Eq. (27) are the altitude z_0 and initial vertical velocity V_{0z} of a pseudo launch point such that the projectile would pass through the current position and target if acted upon only by gravity. Although z_0 is not required for evaluation of Eq. (27), it is included as an unknown such that the problem is fully constrained. These parameters are found as follows. Current altitude, downrange distance, and horizontal velocity are known, such that V_{0x} = current horizontal velocity, and $a = -g$, that is, gravitational acceleration. Launch altitude z_0 and vertical velocity V_{0z} are assumed to be unknown. Eq. (24) is written twice using the ordered pairs $\{x, z\} = \{x, z\}$ and $\{x_t, 0\}$, that is the current state, and target state. The two instances are then rearranged to obtain simultaneous linear equations for the unknown launch altitude and vertical velocity.

$$\begin{bmatrix} 1 & \frac{x}{V_{0x}} \\ 1 & \frac{x_t}{V_{0x}} \end{bmatrix} \begin{Bmatrix} z_0 \\ V_{0z} \end{Bmatrix} = \begin{Bmatrix} z(x) - \frac{a}{2} \left(\frac{x}{V_{0x}} \right)^2 \\ -\frac{a}{2} \left(\frac{x_t}{V_{0x}} \right)^2 \end{Bmatrix} \tag{28}$$

III. Results

III.A. Linear Plant

Preliminary results based on controlling a linear plant with the LTI strategy shown above are shown first. Figure 3 compares the crossrange and altitude of an uncontrolled shot to the Linear Optimal Regulator strategy.

Both shots are aimed with a zero elevation angle to show the drop due to gravity without control. The target is defined as (7582.0,0,0) ft in the gun tube fixed right handed (x, y, z) frame where x points downrange, y to the right, and z points down. The uncontrolled shot impacts the target plane more than 2500 feet left and more than 250 feet below the target. The controlled shot hits within a fraction of a foot in both altitude and crossrange. There is no penalty in this model for lifting controls—no induced drag, and total control effort is not significantly limited. This will not be the case when the test cases are migrated to a full non-linear 6 DOF plant model. To further exercise the algorithm, a Monte Carle set of 50 trajectories

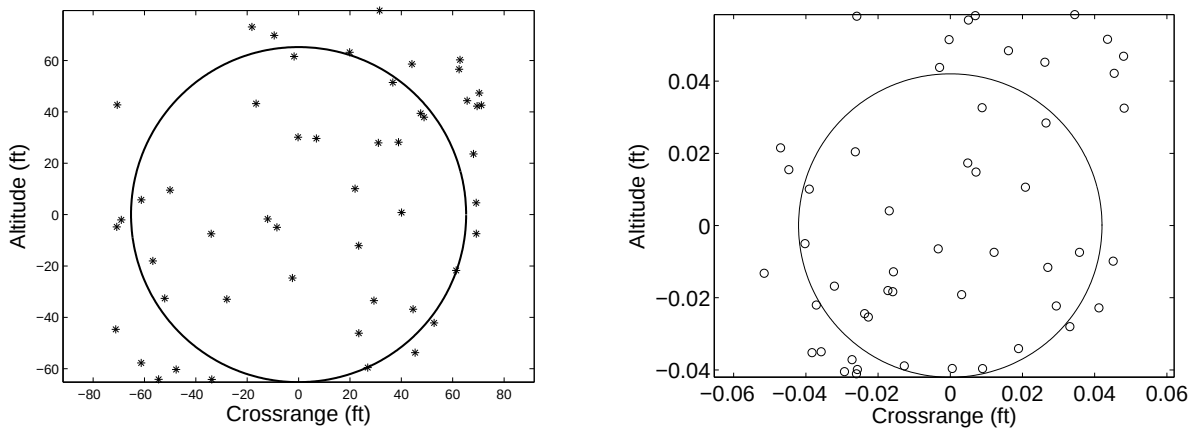

(a) Uncontrolled

(b) Controlled

Figure 4. Comparison of Controlled and Uncontrolled Monte Carlo Dispersion

was simulated. In these preliminary results, the initial pitch and yaw angles were varied according to a uniform distribution with zero mean and standard deviation of 0.594 rad. The set of 50 initial pitch and yaw values was saved such that identical initial conditions were tested with each control strategy.

Figures 4a and b show the uncontrolled and controlled dispersions at the target plane. The CEP circles are drawn in each case such that 50% of the impact points are within the CEP circle. Due to the linear nature of the model and controller, the scatter patterns are identical, and control merely scales down the miss distances in each case.

The performance illustrated here is for ideal conditions only. The plant and control models are linear and identical, and control commands are updated every caliber of downrange travel (35000 updates per trajectory).

III.B. Non–Linear Plant

Performance of the three strategies was tested using a full non–linear 6DOF simulation. Figs 5 and 6 show typical trajectories and canard commands for launches aimed high, low, left and right of target. Differences in the trajectory with and without vacuum correction are not evident at the scaling of Fig. 5.

The Linear Piecewise Time Varying (LPTV) control strategy commands a higher trajectory and tighter crossrange than time invariant cases. Figure 6 shows typical canard deflection in the canard frame for shots aimed above and below ideal. Canard 1 alone is shown to avoid clutter. The depicted oscillations are due to projectile roll—commands in the no–roll frame are rectified and averaged versions of these. Canard 3 would be 180° out of phase with Canard 1 in its local frame such that the pair is in phase in the body frame. Canards 2 and 4 would be similar, to that depicted, just shifted 90° out of phase with Canards 1 and 3 due to their relative position on the rocket. In all cases, the deflections are limited to less than 0.2 rad (11.5°), well within the 1 rad saturation limit enforced.

Again, LTI trajectories appear to be identical regardless of whether or not the vacuum trajectory correction is applied. The controllers are much more active in the low elevation case in order to lift the projectile to a manageable trajectory which reaches the target plane. LPTV produces slightly more aggressive commands early in the trajectory and much smaller amplitudes as the rocket approaches the target.

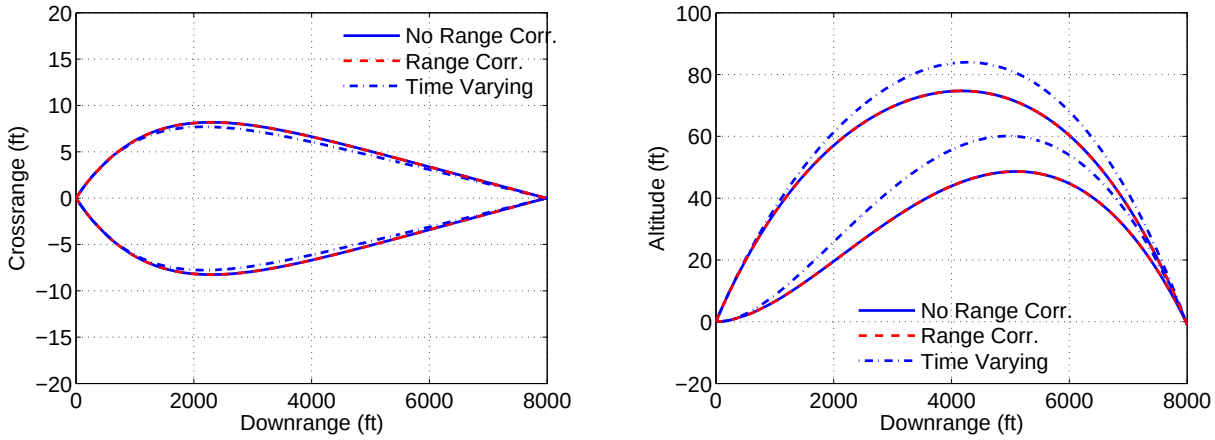

(a) Crossrange

(b) Altitude

Figure 5. Comparison of Controlled Trajectories Using the full Non–Linear Simulation

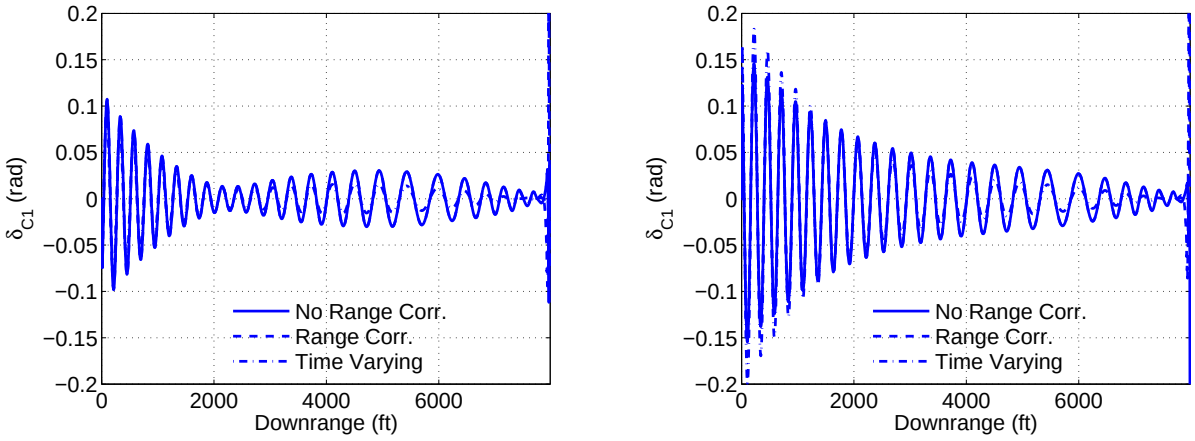

(a) Canard Deflection High Launch Elevation

(b) Canard Deflection Low Launch Elevation

Figure 6. Comparison of Canard Commands Using the full Non–Linear Simulation

Figures 7 and 8 depict dispersion of 50 shots each for the control strategies. All Monte Carlo trials use a common set of pitch and yaw angles at the launch point with mean($\psi \approx 0$) and standard deviation of $\psi \approx 7.78(10^{-3})$ rad. The mean θ is elevated to $3.49(10^{-2})$ rad such that the uncontrolled group is centered at 32.7 ft below the target. θ has a standard deviation of $5.54(10^{-3})$ rad. The uncontrolled dispersion has a CEP of 74.7 ft. One outlier shot at (274.19, 3.30) is not depicted in the plot.

LTI control results shown assume a controller sampling rate of 1 ms. Without vacuum trajectory correction, the CEP is $3.47(10^{-3})$ ft. Clearly there is an altitude bias such that the CEP circle is centered $3(10^{-3})$ ft below the target (altitude is positive down in the dispersion plots).

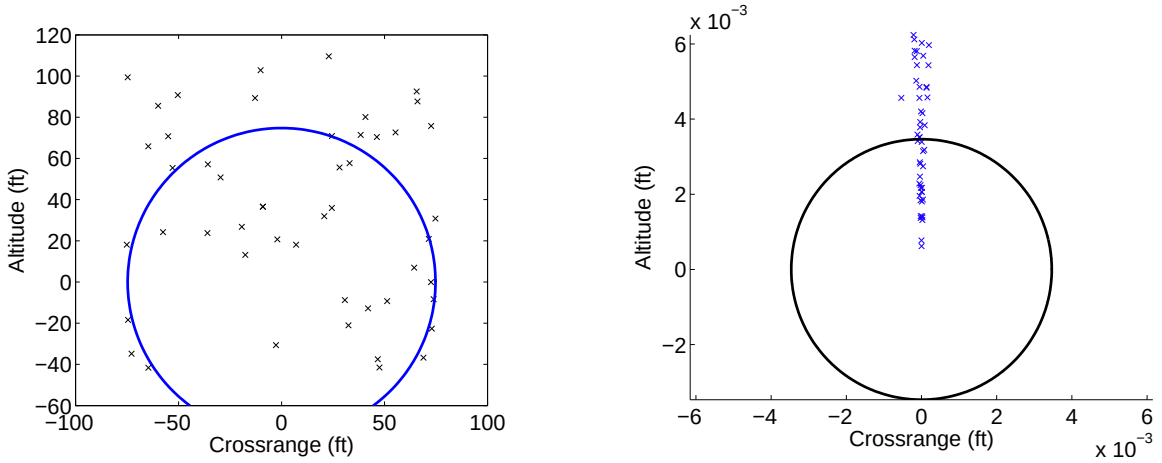

(a) Uncontrolled

(b) LTI Without Range Correction

Figure 7. Dispersion Comparison Using the LTI Controller with Non–Linear Simulation

Including the vacuum trajectory range correction removes much of the altitude bias as shown in Figure 8a. Here the CEP is $1.36(10^{-3})$ft and the group center is near $5(10^{-4})$ft. In both cases, performance is surprisingly good. With control correction every 1 ms, the controller's internal trajectory gets gradually more accurate as the missile flies downrange. The prediction is initially adequate to steer the missile toward the target. As the missile approaches the target, corrections become much more precise. The continuous proportional nature of the canards allows for very precise control near the target plane.

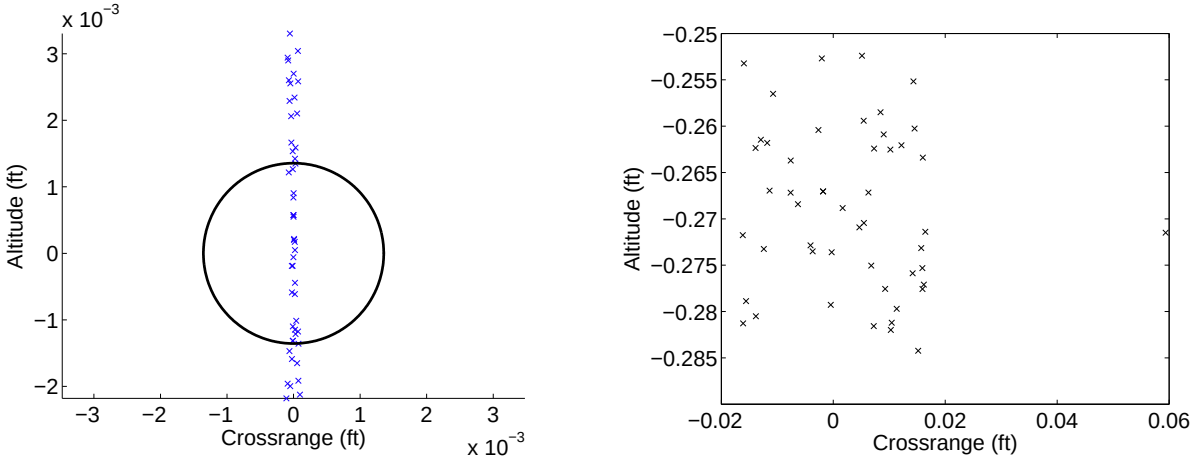

(a) LTI with Vacuum Range Correction

(b) Linear Piecewise Time Varying

Figure 8. Dispersion Comparison Using LTI and LPTV Controllers

Using 50 segments, the LPTV controller yields a CEP of 0.270 ft. This is mostly driven by the group being centered at 0.269 ft above the target as shown in Figure 8b. Apparently the explicit predictions of p

and V contain enough inaccuracy as to be a hindrance for the flat fire trajectories used. Future work will extend this technique to indirect fire trajectories.

The final figures show trade studies on control sampling period (LTI) and number of segments, n_s (LPTV). Without vacuum trajectory range correction, the altitude bias seen earlier dominates CEP such that no clear trend wrt controller sampling period emerges. With vacuum trajectory correction, controller performance is greatly degraded for sampling periods greater than 8 ms.

In the LPTV case, the controller sampling period was held constant at 5 ms. Clearly, performance improves with increased numbers of segments with slightly diminishing returns above $n_s = 40$. Computational burden becomes excessive at $n_s = 50$, so finer segmentation was not tested.

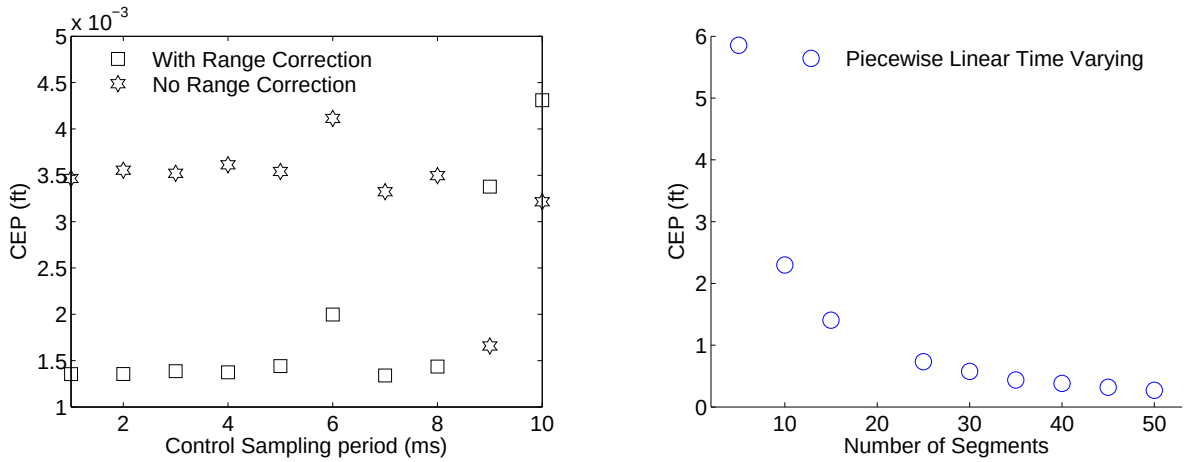

(a) Tine Invariant Controllers

(b) Piecewise Time Varying Controller

Figure 9. Trade Studies of CEP as Control Parameters Vary

IV. Conclusions

Control laws for symmetric projectiles with forward canards have been developed using LTI finite horizon optimal regulator, and LPTV finite horizon regulator. Performance was far superior with the LTI strategy since explicit predictions of roll rate and total velocity were needed for the LPTV strategy. These predictions caused excessive error in the piecewise Riccati equation solution. A correction to downrange distance to go using a target intersecting vacuum point mass trajectory was able to remove much of the altitude bias seen in early trials of the LTI strategy. Future work will involve extending the LPTV method to indirect fire situations where the LTI model breaks down.

References

[1]Burchett, B. T., and Costello, M., "Model Predictive Lateral Pulse Jet Control of an Atmospheric projectile," *Journal of Guidance, Control, and Dynamics*, Vol 25, No. 5, pp. 860-867, September-October 2002.

[2]Ollerenshaw, D., and Costello, M., "Model Predictive Control of a Direct Fire Projectile Equipped with Canards," 2005 AIAA Atmospheric Flight Mechanics Conference, San Francisco, California, 15–18 August, 2005.

[3]Slegers, N. "Predictive Control of a Munition Using Low–Speed Linear Theory," *Journal of Guidance, Control, and Dynamics*, Vol 31, No. 3, pp. 768–775, May–June 2008.

[4]Fresconi, F., and Ilg, M., "Model Predictive Control of Agile Projectiles" 2012 AIAA Atmospheric Flight Mechanics Conference, Minneapolis, Minnesota, 13–16 August, 2012.

[5]Costello, M., Montalvo, C., and Fresconi, F., "MultiBoom: A Generic Multibody Flight Mechanics Simulation Tool for Smart Projectiles," ARL Technical Report No. 6232, October, 2012.

[6]Costello, M., and Peterson, A., "Linear Theory of a Dual-Spin Projectile in Atmospheric Flight," *Journal of Guidance, Control, and Dynamics*, Vol. 23, No. 5, pp. 789–797, September–October 2000.

[7]McCoy, R. L., *Modern Exterior Ballistics*, Schiffer, Atglen, PA, 1999.

[8]Athans, M., Dertouzos, M. L., Spann, R. N., and Mason, S. J., *Systems, Networks, and Computation: Multivariable Methods*, McGraw-Hill, 1974.

[9]Van Loan, C., "Computing integrals involving the matrix exponential," *IEEE Transactions on Automatic Control*, Vol. 23, No. 3, pp. 395-404, 1978.

[10]Burchett, B. T., "Aerodynamic Parameter Identification for Symmetric Projectiles: An Improved Gradient Based Method", AIAA Atmospheric Flight Mechanics Conference, Minneapolis, Minnesota, 13–16 August, 2012, AIAA 2012–4861.

[11]Burchett, B. T., *Robust Lateral Pulse Jet Control of an Atmospheric projectile*, Ph.D. Thesis, Oregon State University, 2001.

[12]Dou, L. and Dou, J., "The Design of Optimal Guidance Law with Multi-constraints Using Block Pulse Functions," *Aerospace Science and Technology*, Vol. 23, No. 1, pp. 201-205, 2012.

Appendix

The integral of Eq. (27) results in

$$\begin{aligned} s_t - s &= \frac{1}{2}\left(\frac{ds}{dx}\Omega V_{0z}V_{0x} + \frac{ds}{dx}\Omega a x \right. \\ &+ \left. a\log_e((V_{0z}V_{0x}a + a^2x + \frac{ds}{dx}V_{0x}^4\Omega)/(V_{0x}^4\Omega))\right)/(a\Omega)\Big|_x^{x_t} \end{aligned} \tag{29}$$

Where ds/dx is defined in Eq. (26), and Ω is given as

$$\Omega = \frac{|a|}{V_{0x}^2}$$